An unsupervised feature extraction and selection strategy for identifying epithelial-mesenchymal transition state metrics in breast cancer and melanoma

David J. Klinke II[1-3] ✉ **and Arezo Torang**[1,4,5]

[1]Department of Chemical and Biomedical Engineering, West Virginia University, Morgantown, WV
[2]Department of Microbiology, Immunology and Cell Biology, West Virginia University, Morgantown, WV
[3]WVU Cancer Institute, West Virginia University, Morgantown, WV
[4]Amsterdam UMC, University of Amsterdam, Laboratory for Experimental Oncology and Radiobiology, Center for Experimental and Molecular Medicine, Cancer Center Amsterdam, Amsterdam, The Netherlands
[5]Oncode Institute, UMC, University of Amsterdam, Amsterdam, The Netherlands

Digital cytometry is opening up new avenues to better understand the heterogeneous cell types present within the tumor microenvironment. While the focus is towards elucidating immune and stromal cells as clinical correlates, there is still a need to better understand how a change in tumor cell phenotype, such as the epithelial-mesenchymal transition, influences the immune contexture. To complement existing digital cytometry methods, our objective was to develop an unsupervised gene signature capturing a change in differentiation state that is tailored to the specific cellular context of breast cancer and melanoma, as a illustrative example. Towards this aim, we used principal component analysis coupled with resampling to develop unsupervised gene expression-based state metrics specific for the cellular context that characterize the state of cellular differentiation within an epithelial to mesenchymal-like state space and independently correlate with metastatic potential. First developed using cell line data, the orthogonal state metrics were refined to exclude the contributions of normal fibroblasts and to provide tissue-level state estimates based on bulk tissue RNAseq measures. The resulting gene expression-based metrics for differentiation state aim to inform a more holistic view of how the malignant cell phenotype influences the immune contexture within the tumor microenvironment.

Epithelial-mesenchymal transition | digital cytometry | deconvolution | transcriptomics

Correspondence: ***david.klinke@mail.wvu.edu***

Introduction

Tissues are comprised of a diverse set of different cell types that help maintain homeostasis. Oncogenesis is associated with a shift in the cellular composition of a tissue that can be revealed with increasing confidence through direct measurement, such as scRNA-seq, or using digital methods to deconvolute bulk tissue samples (1). Given the correlation with response to immunotherapies, the current focus has been on quantifying immune cell types present within the tumor microenvironment (2, 3). There is also an increasing appreciation for characterizing the heterogeneity among malignant cells that may arise in the same anatomical location (4, 5). Given our interest in understanding functional heterogeneity of malignant cells that originate within a particular anatomical organ rather than uncertainty in etiology, we will focus on breast cancer and melanoma as Li et al. show that melanoma and breast cancer cell lines seem to cluster most uniformly while other cell lines defined by anatomical origin seem to have a more heterogeneous composition (6).

While the tumor cells that arise in the skin and breast seem to be most similar, patient treatment strategies and outcomes can be diverse. Initial treatment strategies are guided by specific molecular alterations that can be targeted by drugs: aromatase inhibitors for ER-positive breast cancer, anti-HER2 antibodies for HER2-positive breast cancer, or small molecule inhibitors for BRAF V600E-positive or C-KIT-positive melanoma (7, 8). However, dissemination of primary tumors to vital organs like liver, brain, and lungs is a key limiter for patient survival in breast cancer and melanoma. Specifically, the 5-year survival rate for patients with localized disease versus distant metastases drops from 98% to 23% and from 99% to 27% for melanoma and breast cancer, respectively (9). In contrast, patient survival for tumors that originate in vital organs is limited by the degree to which malignant cells locally disrupt organ function. Thus the importance of distal dissemination in determining patient outcomes can vary based on the tissue of origin.

The distal dissemination and growth of malignant cells - metastasis - is a complex process thought to involve dynamic re-engagement of biological processes used during development that enable migrating cells to form tissues. For carcinomas, initiating metastasis is thought to occur through a process called the epithelial-mesenchymal transition (EMT). EMT is the functional consequence of engaging a genetic regulatory network that downregulates the expression of genes associated with an epithelial phenotype and upregulates genes associated with a mesenchymal phenotype. Breast carcinoma primarily originates from either luminal epithelial cells or basal myoepithelial cells within the mammary gland (10). In contrast to breast cancer, melanoma arises from the oncogenic transformation of melanocytes, which follow a different developmental trajectory along the neural crest than epithelial cells but also involves a process similar to EMT (11). While much of cell specification is imprinted epigenetically via DNA methylation and histone modifications, significant functional changes, such modifications in cell state due to EMT, may occur within these epigenetic constraints. To characterize cell state based on gene expression, supervised methods have been predominantly used for developing gene signatures that characterize the epithelial-mesenchymal transition. While effective, supervised methods can perform poorly if the strategy is based on misinformation, such as sample misclassification or prior biases as to the number of cell states or defining genes. While used less frequently, unsupervised methods for feature extraction and selection are advantageous as they can be data-driven (12). Here, our objective was to develop an unsupervised gene signature capturing this change in phenotype that is tailored to the specific cellular context of breast cancer and melanoma, as a illustrative example.

Results

RNA-sequencing provides an estimate of protein abundance. We first asked whether assaying the same genes using different transcriptomics profiling platforms provides the same information. To do this, we compared gene expression levels assayed by either Agilent microarray or by Illumina RNA-sequencing for the same samples (Figure 1). Expression values obtained by RNA-seq are in units of transcripts per million (TPM) while the Agilent Microarray results are in terms of intensity units. Using samples obtained as part of the breast cancer arm of the TCGA, we focused on genes that have been associated with host immunity, as these genes are likely to span a broad dynamic range within these samples. As the TCGA samples are obtained from homogenized bulk samples of tumor and matched normal breast tissue, expression of these genes could be from the malignant cells, like GATA3 expression by breast cancer cells, or from immune cell infiltrates, like the potential expression of IL4 and IL5 by infiltrating T helper type 2 cells.

Generally, comparing the same row across the two panels illustrates the poor correspondence between intensity units and read counts (TPM). A subset of genes, like HLA-DRA and HLA-DPA1, exhibit both high microarray intensity units and read counts while other genes, like TBX21 and FASLG, exhibit high microarray intensity units but have low read counts. In addition, the dynamic range observed among these samples is different depending on the platform used, as illustrated in the heatmap by TBX21 and IL17F. Using Illumina RNAseq, TBX21 is constrained to the low end of the color spectrum (dark to royal blue) while the dynamic range spans the middle to upper end of the color spectrum (green to red) when assayed using Agilent microarray. Similarly, IL17F transcripts were not detected by RNA-seq in 87% of the samples but the Agilent microarray shows a rather high average intensity with variation among the samples. The difference in average intensities among genes and in variance among samples assayed by these two platforms suggest that the information provided by these two platforms is not entirely the same.

We next asked whether the observed transcript abundance observed by RNA-seq corresponds to protein abundance. For this, we compared RNA-seq counts reported for cell lines associated with the Cancer Cell Line Encyclopedia with protein abundance for the same cell lines measured using Reverse Phase Protein Array (RPPA). We filtered the respective data sets to those cell lines that were reported in both data sets and for genes where there was a positive correlation coefficient greater than 0.36 between read counts in RPKM and normalized RPPA values. From the initial data sets, 283 cell lines and 147 genes were retained for analysis after filtering. Next, we determined whether the pairs of mRNA and protein measurements share a common value for steady-state transcript abundance that corresponds to steady-state protein abundance measured above background. To do this, we applied a protein expression model to each gene measured across the cell lines where protein abundance was assumed to be a saturable function of transcript abundance (Fig. 2A). Using the fitted curve, the threshold of transcript reads for detecting a change in protein abundance 2.5% above background was back calculated. Example data sets and the corresponding curve fits for the genes CLDN7, AXL, JAG1, and CDH1 are shown in Figure 2B. Interestingly, the maximum value in the distribution in calculated threshold values corresponded to 1 RPKM (Fig 2C). As the average intensity units and read counts (TPM) for a given gene across samples do not correlate, these results imply that the average intensity obtained by microarray does not correlate with protein abundance.

Collectively, this common threshold value has two implications. First, there are some genes that have a high sensitivity of detection using Agilent microarrays such that the observed changes may not be functionally important. From Figure 1, it seems that IL17F, TBX21, FASLG, KLRD1, IFNG, CCL17, and IL10 are but a few examples (i.e., high microarray intensity but very low read counts) in that dataset. Without knowing the detection sensitivity by microarray, traditional approaches using a z-score metric may give equal weight to changes in gene expression driven by a biological signal as to changes dominated by random noise. Second, the threshold value provides a rationale for filtering genes that are likely to have a low information content when developing gene signatures for phenotypes that are not well defined.

Gene expression patterns in breast cancer cells are captured by a single component. Given the variety of breast cancer subtypes reported in the literature, we next asked how many different genetic regulatory networks (GRN) are at work in breast cancer. GRNs associated with development commonly contain transcription factors that interact via positive feedback such that the target genes are either co-expressed or expressed in a mutually exclusive fashion (13). Given the interest in functional responses, we are focusing on patterns of gene expression in response to signal processing by the genetic regulatory network rather than trying to identify the topology of the GRNs. In motivating this study, we made four assumptions. First, we assumed that oncogenic mutations alter the peripheral control of GRN but do not alter the core network topology, where signals processed by a GRN change cell phenotype by engaging a unique gene expression pattern. Second, malignant cells derived from a particular anatomically-defined cancer represent the diverse ways that hijacking these GRNs can provide a fitness advantage to malignant cells within the tumor microenvironment. Third, culturable tumor cell lines represent a sampling of these ways in which GRNs are hijacked in a particular anatomical location. Fourth, the process of isolating these malignant cells from tumor tissue to generate culturable cell lines does not bias this view. It follows then that the number of different GRNs can be identified by analyzing the transcriptional patterns of genes likely to participate in GRNs among an ensemble of tumor cells lines that share a common tissue of origin. We focused our attention on 780 genes that have been previously associated with the epithelial-mesenchymal transition and related Gene sets in MSigDB v4.0. and analyzed the expression of these genes among breast cancer cell lines included in the CCLE database as assayed by RNA-sequencing using a workflow summarized in Figure 3. To identify coordinately expressed genes, we used Principal Component Analysis (PCA), a linear statistical approach for unsupervised feature extraction and selection that enables the unbiased discovery of clusters of genes that exhibit coherent patterns of expression (i.e., features) that are independent of other gene clusters (14). The relative magnitude of the resulting gene expression patterns can be inferred from the eigenvalues, which is shown in Figure 4. Specifically, PC1 and PC2 captured 65% and 14% of the variance, respectively. Additional principal components each captured less than 4% of the variance.

One of the challenges with PCA is that no clear rules exist to determine how many principal components to consider, such as a gap statistic in clustering (15). To select an appropriate number of PCs (i.e., features), we established a threshold for determining significance relative to a null distribution. Specifically, we applied the same PCA to a synthetic noise dataset generated from the original data by randomly resampling with replacement the collection of gene expression values and assigning the values to particular gene-cell line combinations. The resulting set of eigenvalues represent the values that could be obtained by random chance if the underlying dataset has no information, which are shown as the dotted red line in Figure 4A. In comparison to the null distribution, only the first two PC were above the threshold. The variance captured by the remaining PCs were below the null PCA distribution suggesting that any potential biological interpretations of these additional PCs could also be explained by random chance. Therefore we focused on the first two PCs.

As variance in read counts is proportional to abundance, gene projections along the PC1 axis were proportional to the average read counts of the corresponding gene among the samples. Measured transcript abundance is proportional to the basal gene expression associated with cell specification and technical artifacts associated with RNA sequencing. Genes were retained for further analysis that were expressed above the 1 RPKM threshold in more that 5% of the cell lines. Next, we focused on the projection of retained genes along principal components 2 and 3. The projections were annotated with horizontal and vertical dotted lines that enclose 95% of the projections from the null distribution. While the majority of the genes were distributed around the origin, a subset of genes were projected along the extreme of the PC2 axis (outside of the dotted vertical lines) and had no significant projection along the PC3 axis (inside of the dotted horizontal lines). The list of genes associated with either the high PC2/null PC3 or the low PC2/null PC3 groups are listed in Supplemental Table S1 and contained 128 and 101 genes, respectively. As the projection of Vimentin (VIM - yellow dot in Figure 4C) and E-cadherin (CDH1 - blue dot in Figure 4C) were prototypical for these two groups of genes, the high PC2/null PC3 genes were annotated as a mesenchymal signature (i.e., a de-differentiated state) genes and the low PC2/null PC3 group were annotated as an epithelial signature (i.e., a terminally differentiated state). In contrast to supervised approaches that use Vimentin and E-cadherin as the basis to identify associated genes (e.g., (16, 17)), the approach used here is unsupervised whereby the association of Vimentin and E-cadherin with these two opposite groups of genes emerges naturally from the data.

The Epithelial and Mesenchymal state measures stratify intrinsic subtypes of breast cancer and metastatic potential. Using these two sets of genes, we developed a state metric to quantify the extent of a gene expression signature associated with epithelial differentiation and mesenchymal de-differentiation using a normalized sum over all of the genes associated with a signature. While the PCA results suggest that these two sets of genes are inversely related, the metrics were designed to represent each state independently such that cells that exhibit a pure phenotype would have values of 1 and 0 associated with their respective state metrics and cells with mixed phenotypes could potentially have values of 1 for both state metrics. Next we calculated the state metric values for all of the breast cancer cell lines, where their projections in state space are shown in Figure 5. Interestingly, the breast cancer cell lines largely followed a linear reciprocal relationship between epithelial (E) and mesenchymal (M) states (dotted line in Figure 5) and were segregated by intrinsic PAM50 subtype (18). While HER2, Luminal A, Luminal B, and Basal subtypes all have a high E signature, they progressively increased in their M signature. The Claudin Low subset spanned the greatest range with some expressing a high E and moderate M signatures (e.g., HCC1569, MDAMB361, HMEL) and others with a low E and high M signatures (e.g., BT549 and HS578T). Of note, a subset of the Claudin Low cell lines (e.g., HS742T, HS343T, HS281T, HS606T, and HS274T) with high M and very low E signatures have been suggested by the CCLE to be fibroblast-like (see Cell_lines_annotations_20181226.txt). Functionally, cells with low E and high M signatures had a high propensity for metastasis while the propensity for metastasis was low in cell lines with high E and low M signatures

(19).

We next assessed the epithelial and mesenchymal state metrics in breast cancer cells assayed using scRNA-seq (20) (see Figure 5B). Similar to the cell lines, the samples were spread across the epithelial to mesenchymal spectrum roughly ordered by their corresponding intrinsic subtype, where HER2 subtype had a high E/low M signature and the basal subtype had the highest M signature without much of a reduction in their E signature. Overall the state values were farther below the reciprocal trendline than any of the cell line sampled. As gene-level reads by scRNA-seq are frequently missing (i.e., a dropout read)(21), we imputed missing values to assess whether the distribution in the E/M state values were a result of read dropouts (see Figure 5C). While read imputation shifted the cell state metrics toward the reciprocal trendline, the heterogeneity among the cell measurements was lost. Overall, it is unclear whether scRNA-seq measurements can be used to identify biological heterogeneity separately from heterogeneity introduced by technical limits of the assay.

While single-cell methods are rapidly emerging as tool to assay human tissue samples, bulk transcriptomic assays of tumor tissue samples, like those acquired as part of the Cancer Genome Atlas are more abundant. More samples increases the statistical power for identifying clinical, cellular, and genetic correlates of the epithelial-mesenchymal transition. However, applying the epithelial/mesenchymal state metrics to interpret RNA-seq assays of bulk tumor tissue samples requires some additional filtering steps as bulk RNA-seq measurements averages over the heterogeneous normal and malignant cell types present within the tissue. In terms of a gene signature for the epithelial-mesenchymal transition, many of the genes commonly associated with acquiring mesenchymal function are associated with fibroblasts, a relatively common cell type in epithelial tissues. Thus, an enrichment of genes associated with the epithelial-mesenchymal transition may be explained solely by a shift in the prevalence of fibroblasts within the tissue sample. To deconvolute fibroblast genes from the state metrics, we obtained a list of 2500 genes that were uniquely associated (Area under ROC curve > 0.5) with a cluster annotated as fibroblasts using scRNAseq data obtained from a digested normal skin sample obtained human female. This cluster contained about 1/3 of the cell samples measured within the CD45-negative population of the digested skin sample (see Supplemental Figure S1). Using this fibroblast gene list, overlapping genes were removed from the state metrics and highlighted in yellow in Supplemental Table S1. All but one of the genes removed were contained within the mesenchymal gene list.

Gene expression assayed from a bulk tissue sample reflects the combined contributions of non-malignant cells plus the changes induced by oncogenic transformation, and reciprocal changes due to de-differentiation among malignant cells. Observable changes depend on the relative contributions of each cell source. As the unsupervised PCA analysis of the cell line data suggested that genes associated with EMT can be revealed by identifying a reciprocal pattern of gene expression, we performed Ridge logistic regression using the sample annotation to obtain regression coefficients for the list of EMT genes that passed the fibroblast filter (n = 158). The regression coefficients were used to filter the list of EMT genes for consistency with the reciprocal gene signature identified in the CCLE analysis. Genes that passed the consistency filter were used to define the epithelial and mesenchymal state metrics for bulk tissue samples. Of note, E-cadherin (CDH1) and CEACAM1 were associated with the epithelial state metric while N-cadherin (CDH2), Wnt-inducible signaling pathway protein 1 (WISP1/CCN4), and matrix metallopeptidase 3 (MMP3) were associated with the mesenchymal state metric. The list of genes associated with the corresponding state metrics are summarized in Supplemental Table S2.

Next, we projected the BRCA tissue samples in EMT space using the two tissue-based state metrics. Similar to the CCLE analysis, all samples clustered along the reciprocal SM_E versus SM_M line but exhibited greater dispersion. Samples obtained from normal breast tissue clustered separately from breast cancer samples (Figure 6), with normal breast tissue samples having the highest values for the epithelial state and lower values, on average, for the mesenchymal state. Among the different clinical breast cancer subtypes, the median value for SM_E progressively decreased from ER/PR+ (luminal), HER2+, and triple negative (TN: ER-/PR-/HER2-) subtypes. The mesenchymal projections were for both ER/PR+ and HER2+ subsets were about equal and higher than the TN samples. We note that, while the HER2+ samples were roughly equal to the ER/PR+ along the SM_M axis, the HER2+ samples were lower than the ER/PR+ samples along the SM_E axis, which aligns with clinical observations. For instance, patients with HER2+ subtype of breast cancer are at increased risk for developing metastatic lesions compared to TN and luminal subtypes (22). The two different state metrics seem to capture gene signatures that help anchor a cell to it's designated location within the tissue and that promotes active migration, respectively. In other words, reducing SM_E corresponds to raising the anchor and increasing SM_M corresponds to hoisting the sail. In summary, both cell-level and tissue-level EMT state metrics provide an estimate of metastatic potential and a digital measure of malignant cell differentiation state in the context of breast cancer.

Gene expression patterns in melanoma cells are also captured by a single component. Using the same workflow as the breast cancer analysis (Figure 3), we applied principal component analysis to the expression of EMT-related genes assayed in an ensemble of XX melanoma cell lines associated with the Cancer Cell Line Encyclopedia (Figure 7). We focused on the first two principal components, PC1 and PC2, that captured 80% and 6% of the variance, respectively. Additional principal components each captured less than 4% of the variance. PC1 captured the variance associated with read abundance, as gene projections along the PC1 axis were proportional to the average read counts among the samples. Vimentin (VIM) and fibronectin (FN1) were two of the most highly expressed genes while members of the Wnt family were some of the genes with low expression (e.g., WNT1, WNT6, WNT8B, WNT3A, WNT8A, WNT9B). Genes retained for further analysis were expressed above the 1 RPKM threshold in more than 5% of the cell lines.

Next, we focused on the projection of retained genes along PC2 and PC3 axes. The projections were annotated with horizontal and vertical dotted lines that enclose 95% of the projections from the null distribution. While the majority of the genes were distributed around the origin, a subset of genes were projected along the extreme of the PC2 axis (outside of the dotted vertical lines) and had no significant projection along the PC3 axis (inside of the dotted horizontal lines). The list of genes associated with either the high PC2/null PC3 or the low PC2/null PC3 groups are listed in Supplemental Table S1 and contained 26 and 90 genes, respectively. In contrast to the breast cancer results, the projection of Vimentin (VIM - yellow dot in Figure 7C) and E-cadherin (CDH1 - blue dot in Figure 7C) were not associated with either of these two groups of genes. As the high PC2/null PC3 group included MITF, a master regulator of melanocyte differentiation, and the low PC2/null PC3 group included a number of EMT-related genes (e.g., FN1, TCF4, ZEB1, TWIST2, and WISP1), these two gene sets were annotated as a terminally differentiated signature (i.e., an epithelial-like state) and a de-differentiated signature (i.e., a mesenchymal-like state), respectively.

Projections of the melanoma cell lines in differentiation state space were calculated using the two gene signatures (Figure 8). Similar to the breast cancer cell lines, the melanoma cell lines largely followed a linear reciprocal relationship between terminally differentiated (SM_T) and de-differentiated (SM_D) states (dotted line in Figure 8). The majority of cell lines exhibited primarily a terminally differentiated signature with some expression of de-differentiated genes while only a small subset of the cell lines exhibited primarily a de-differentiated signature. The gene signatures for single melanoma cells were also highly heterogeneous due to dropout of gene reads.

Using state metrics refined for use with tissue samples (see Supplemental Table S2), samples acquired from benign melanocytic nevi and untreated primary melanoma tissue were projected onto the state space. Of note, CEACAM1 and MITF were associated with the differentiated state and three genes - CEACAM1, CGN, and HPGD - were shared with the breast cancer epithelial state metric. The de-differentiated state metric had five genes - WISP1/CCN4, EDNRA, FOXC2, SERPINE1, and SPOCK1 that were shared with the breast cancer mesenchymal state metric. While samples were more narrowly distributed in state space compared to the cell lines (Figure 9), all of the benign nevi exhibited higher terminally differentiated (SM_T) and tended to have lower de-differentiated values (SM_D). The samples from primary melanoma were color-coded based on the annotated Breslow's depth, where higher values were associated with lower terminal differentiation scores. Using Breslow's depth as a surrogate measure of metastatic potential (23), tissue-level EMT state metrics provide an estimate of metastatic potential and a digital measure of malignant cell differentiation state in the context of melanoma.

Terminal differentiation is associated with distinct gene signatures while de-differentiation seems to engage common gene regulatory networks. The separate gene signatures generated for breast cancer cells and melanoma cells using an unsupervised approach provide an opportunity to identify unique and shared aspects of the genetic regulatory mechanisms underpinning cell specification, as summarized in Figure 9. Specifically, we used DAVID to identify genes with transcription factor activity using the GOTERM_MF_ALL: Sequence_specific_DNA_binding + UP_Keywords:DNA_binding. In the breast cancer cell lines, nine transcription factors were upregulated in cells with a terminally differentiated phenotype, including GRHL2 and OVOL2 that have been associated with enforcing epithelial differentiation (24). Correspondingly, five transcription factors were upregulated in melanoma cells, including MITF that is essential for melanocyte differentiation (25). Interestingly, there was no overlap in the genes with transcription factor activity in the two differentiated cell signatures. In contrast, melanoma and breast cancer cell lines that exhibited a de-differentiated phenotype shared five transcription factors, including TWIST2 and ZEB1. De-differentiation in breast cancer cell lines were also associated with an additional six transcription factors, including TWIST1 (26). Overall, the analysis of these transcription factors is consistent with specificity in phenotype as a consequence of engaging gene regulatory networks unique to a specialized cell subset while de-differentiation seemed to engage common gene regulatory networks that facilitate the loss of cell specificity.

Discussion

Here we used an unsupervised feature extraction and selection approach based on principal component analysis and resampling to identify state metrics for the epithelial-mesenchymal transition in breast cancer and melanoma. Given the importance for identifying patients with tumors likely to metastasize, a number of gene signatures have been developed to predict the prevalence of tumor cells with a epithelial-mesenchymal transition signature (16, 17, 27–29). Supervised approaches are most common (16, 17, 27, 28), where samples are classified a priori. For instance, Koplev et al. (28) develop gene signatures that average over all anatomical locations while Levine and coworkers (27, 30) classify training samples a priori into one of three cell states: epithelial, mesenchymal, or hybrid E/M. Rokavec et al. generate features based on co-expression with E-cadherin and Vimentin (17). While effective, supervised methods can perform poorly if the strategy is based on misinformation, such as sample misclassification or prior biases as to the number of cell states or defining genes. We also note that state metrics developed using microarray technology (e.g., (16)) are not likely relevant for interpreting data based on RNA sequencing, given the unclear relation between transcriptome and protein abundance as assayed using microarray technology. While rarely used, the data-driven nature of unsupervised methods for feature extraction and selection are attractive (12). For instance, Umeyama et al. used an unsupervised approach for feature extraction to identify genes associated with metastasis (31). To illustrate this data-driven approach, we have focused on breast cancer and melanoma, where metastatic dissemination to vital organs are key limiters of patient survival. In summary, we hope that our developed state metrics find use alongside other digital cytometry tools to better understand how oncogenic transformation alters the immune contexture within the tumor microenvironment.

Methods

'Omics Data. Transcriptomics profiling of the same samples using both Agilent microarray and Illumina RNA sequencing for the breast cancer arm (BRCA) of the Cancer Genome Atlas was downloaded from TCGA data commons. Values for gene expression, expressed in RPKM, for the cell lines contained within the Cancer Cell Line Encyclopedia were downloaded from the Broad data commons (Website: https://portals.broadinstitute.org/ccle File: CCLE_RNAseq_081117.rpkm.gct accessed 12/22/2017). Reverse phase protein array (RPPA) results for the cancer cell lines were obtained from the M.D. Anderson proteomics website (Website: https://tcpaportal.org/mclp/ File: MCLP-v1.1-Level4.txt accessed 6/15/2018) (6). Single-cell gene expression (scRNA-seq) for breast cancer and melanoma cells expressed in TPM were downloaded from the Gene Expression Omnibus (GEO) entries GSE75688 and GSE72056, respectively. 10X Genomics scRNA-seq data for CD45-negative cells digested from a normal human female skin sample and expressed in counts of gene-level features was downloaded from European Bioinformatics Institute (EMBL-EBI) ArrayExpress entry E-MTAB-6831. RNAseq data expressed in counts assayed in samples acquired from benign melanocytic nevi and untreated primary melanoma tissue and associated annotation were downloaded from GEO entry GSE98394.

Non-linear regression of protein abundance to mRNA expression. All data was analyzed in R (V3.5.1) using the 'stats' package (V3.5.1). For each gene where complementary CCLE and RPPA data exist and for which their correlation coefficient was above 0.36, the non-linear function,

$$Y_{protein} = a + \frac{b \cdot X_{mRNA}}{X_{mRNA} + c}, \tag{1}$$

was regressed using the *nls* function to the resulting protein ($Y_{protein}$) and transcript (X_{mRNA}) abundance data. As the RPPA values are normalized, the parameters a and b represent the background value and maximum detectable increase above background, respectively, while the parameter c represents the midpoint in transcript abundance within the dynamic range of the assay. A minimum in the summed squared errors between model-predicted and observed RPPA values were used to determine the optimal values of the model parameters. Using the optimal values, a threshold was estimated independently for each gene based on the transcript abundance that yields a 2.5% increase in protein abundance above background.

Statistical analysis for cell-level signatures. Principal component analysis (PCA) was performed on log base 2 transformed RPKM values using the *prcomp* function on the CCLE RNA-seq data, which was filtered to 780 genes previously associated with epithelial-mesenchymal transition. The collective list of genes were assembled from prior studies (16, 32–36) and additional gene sets from MSigDB V4.0 including: “EPITHELIAL TO MESENCHYMAL TRANSITION" and “REACTOME TGF BETA RECEPTOR SIGNALING IN EMT EPITHELIAL TO MESENCHYMAL TRANSITION". PCA was applied to the genes to extract the features, where the resulting eigenvectors capture the relative influence of a gene's expression on a specific principal component and the eigenvalues represent how much information contained within the dataset is captured by a specific principal component. Drawing upon conventional hypothesis testing where significance is established by rejecting the null hypothesis that experimental observations could be explained by random chance, we used a resampling approach to establish a null hypothesis related to the eigenvalues, that is to determine the true rank of the noisy expression matrix. The resampling approach involved repetitively applying PCA (n = 1000) to a synthetic noise dataset with the same dimensions that was generated from the original data by randomly resampling with replacement from the collection of gene expression values and assigning the values to particular gene-cell line combinations. The resulting distribution of eigenvalues and eigenvectors represent the values that could be obtained by random chance if the underlying dataset has no information (i.e., the null PCA distribution). Principal components with eigenvalues greater than the null PCA distribution were used to define the principal subspace for subsequent analysis, that is the selection of features. Similarly, the distribution in the projection of genes within the null PCA space were used to determine whether the projection of a gene along a particular PC axis was explained by random chance or not by setting thresholds along the PC2 and PC3 axes that enclosed 95% of the null PCA space. The PC projection of genes relative to the null PCA space was used to refine the extracted features.

A metric was developed to estimate the extent that a cell exhibits a gene signature corresponding to a “Epithelial/Terminally Differentiated" versus “Mesenchymal/Dedifferentiated" state. The state metrics (SM) quantify the cellular state by averaging over a normalized expression level of each gene in the signature ($reads_i$, expressed in TPM) according to the formula:

$$SM = \frac{1}{n_{gs}} \sum_{i=1}^{n_{gs}} \frac{reads_i}{reads_i + 2^{K_i}}. \tag{2}$$

The genes included in a signature with their corresponding

K_i values are listed in Supplemental Table S1 and n_{gs} corresponds to the number of genes within a signature. The K_i values were estimated by clustering the log2 expression of each gene into two groups using the k-means method and the value was set as the mid-point in expression between the two groups.

Statistical analysis for tissue-level signatures. Genes differentially expressed in normal epithelial fibroblasts were obtained by analyzing single-cell RNAseq data of normal skin obtained using a Genomics 10x platform and a bioinformatics workflow based on the scater (V1.12.2) and SC3 (V1.12.0) packages in R. Briefly, scRNAseq data were filtered to retain samples that had less than 50% of the reads in the top 50 genes and to remove outlier samples based on PCA analysis. Gene-level features were limited to those that were expressed at greater than 1 count in more than 10 cell samples. Read depth was normalized using a variant of CPM contained within the *scran* (V1.12.1) package, which develops a sample-specific normalization factor repetitive sample pooling followed by deconvoluting a sample-specific factor by linear algebra. Following from Davidson et al. (37), fibroblasts were annotated based on co-expression of COL1A1 and COL1A2. Samples were clustered and genes differentially associated with each cluster were identified using the *SC3* workflow (V1.14.0) using default parameters (see Figure S1).

Prior to logistic regression analysis, TCGA BRCA data and the benign nevi and melanoma data were filtered to remove sample outliers and normalized based on housekeeping gene expression (38). Using normal versus tumor annotation associated with the data, ridge logistic regression was performed on log base 2 transformed TPM and median-centered values using the *glmnet* package (V2.0-18), which was limited to EMT-related genes identified in the CCLE analysis and not associated with normal fibroblasts. To minimize overfitting, ridge logistic regression was repeated 500 times using a subsample of the original data set using the genes associated with each signature separately. In each iteration, the samples were randomly assigned in an 80:20 ratio between training and testing samples. Regression coefficients were captured for each iteration using a lambda value that minimized the misclassification error of a binomial prediction model estimated by cross-validation. Accuracy was assessed using the testing samples. Genes were determined to have a consistent expression pattern if greater than 95% of the distribution in regression coefficients had the correct sign. Similarly to the cell-level analysis, state metrics were developed for bulk tissue-level RNAseq measurements to estimate the extent that a tissue sample exhibits a gene signature corresponding to a “Epithelial/Terminally Differentiated" versus “Mesenchymal/De-differentiated" state. The genes included in a signature and their corresponding K_i values are listed in Supplemental Table S2.

ACKNOWLEDGEMENTS

This work was supported by National Science Foundation (NSF CBET-1644932 to DJK) and National Cancer Institute (NCI 1R01CA193473 to DJK). The content is solely the responsibility of the authors and does not necessarily represent the official views of the NSF or NCI.

AUTHOR CONTRIBUTIONS

These contributions follow the International Committee of Medical Journal Editors guidelines: http://www.icmje.org/recommendations/. Conceptualization: DJK; Study Design: DJK; AT;; Data Analysis: DJK; AT; Data Interpretation: DJK; Funding acquisition: DJK; Methodology: DJK; AT; Project administration: DJK; Software: DJK; AT; Supervision: DJK; Writing – original draft: DJK; Writing – review & editing: all authors.

COMPETING FINANCIAL INTERESTS

The authors declare no competing financial interests.

Bibliography

1. A. M. Newman, C. B. Steen, C. L. Liu, A. J. Gentles, A. A. Chaudhuri, F. Scherer, M. S. Khodadoust, M. S. Esfahani, B. A. Luca, D. Steiner, M. Diehn, and A. A. Alizadeh. Determining cell type abundance and expression from bulk tissues with digital cytometry. *Nat. Biotechnol.*, May 2019.
2. V. Thorsson, D. L. Gibbs, S. D. Brown, D. Wolf, D. S. Bortone, T. H. Ou Yang, E. Porta-Pardo, G. F. Gao, C. L. Plaisier, J. A. Eddy, E. Ziv, A. C. Culhane, E. O. Paull, I. K. A. Sivakumar, A. J. Gentles, R. Malhotra, F. Farshidfar, A. Colaprico, J. S. Parker, L. E. Mose, N. S. Vo, J. Liu, Y. Liu, J. Rader, V. Dhankani, S. M. Reynolds, R. Bowlby, A. Califano, A. D. Cherniack, D. Anastassiou, D. Bedognetti, A. Rao, K. Chen, A. Krasnitz, H. Hu, T. M. Malta, H. Noushmehr, C. S. Pedamallu, S. Bullman, A. I. Ojesina, A. Lamb, W. Zhou, H. Shen, T. K. Choueiri, J. N. Weinstein, J. Guinney, J. Saltz, and et al. The Immune Landscape of Cancer. *Immunity*, 48(4):812–830, 04 2018.
3. I. Tirosh, B. Izar, S. M. Prakadan, M. H. Wadsworth, D. Treacy, J. J. Trombetta, A. Rotem, C. Rodman, C. Lian, G. Murphy, M. Fallahi-Sichani, K. Dutton-Regester, J. R. Lin, O. Cohen, P. Shah, D. Lu, A. S. Genshaft, T. K. Hughes, C. G. Ziegler, S. W. Kazer, A. Gaillard, K. E. Kolb, A. C. Villani, C. M. Johannessen, A. Y. Andreev, E. M. Van Allen, M. Bertagnolli, P. K. Sorger, R. J. Sullivan, K. T. Flaherty, D. T. Frederick, J. Jane-Valbuena, C. H. Yoon, O. Rozenblatt-Rosen, A. K. Shalek, A. Regev, and L. A. Garraway. Dissecting the multicellular ecosystem of metastatic melanoma by single-cell RNA-seq. *Science*, 352(6282): 189–196, Apr 2016.
4. B. Shannan, M. Perego, R. Somasundaram, and M. Herlyn. Heterogeneity in Melanoma. *Cancer Treat. Res.*, 167:1–15, 2016.
5. S. Koren and M. Bentires-Alj. Breast Tumor Heterogeneity: Source of Fitness, Hurdle for Therapy. *Mol. Cell*, 60(4):537–546, Nov 2015.
6. J. Li, W. Zhao, R. Akbani, W. Liu, Z. Ju, S. Ling, C. P. Vellano, P. Roebuck, Q. Yu, A. K. Eterovic, L. A. Byers, M. A. Davies, W. Deng, Y. N. Gopal, G. Chen, E. M. von Euw, D. Slamon, D. Conklin, J. V. Heymach, A. F. Gazdar, J. D. Minna, J. N. Myers, Y. Lu, G. B. Mills, and H. Liang. Characterization of Human Cancer Cell Lines by Reverse-phase Protein Arrays. *Cancer Cell*, 31(2):225–239, 02 2017.
7. A. Taghian, M. D. El-Ghamry, and S. D. Merajver. Overview of the treatment of newly diagnosed, non-metastatic breast cancer. *UpToDate*, 2019.
8. J.A. Sosman. Overview of the management of advanced cutaneous melanoma. *UpToDate*, 2019.
9. American Cancer Society. *Cancer Facts & Figures 2019*. American Cancer Society, Atlanta, Ga, 2019.
10. M. Zhang, A. V. Lee, and J. M. Rosen. The Cellular Origin and Evolution of Breast Cancer. *Cold Spring Harb Perspect Med*, 7(3), Mar 2017.
11. T. Regad. Molecular and cellular pathogenesis of melanoma initiation and progression. *Cell. Mol. Life Sci.*, 70(21):4055–4065, Nov 2013.
12. Y. H. Taguchi. Principal Components Analysis Based Unsupervised Feature Extraction Applied to Gene Expression Analysis of Blood from Dengue Haemorrhagic Fever Patients. *Sci Rep*, 7:44016, 03 2017.
13. Uri Alon. *An introduction to systems biology: design principles of biological circuits*, volume 10 of *Chapman & Hall/CRC mathematical and computational biology series*. Chapman & Hall/CRC, Boca Raton, FL, 2007.
14. I. T. Jolliffe and J. Cadima. Principal component analysis: a review and recent developments. *Philos Trans A Math Phys Eng Sci*, 374(2065):20150202, Apr 2016.
15. R. Tibshirani, G. Walther, and T. Hastie. Estimating the number of clusters in a data set via the gap statistic. *J. R. Statist. Soc. B.*, 63(2):411–423, 2001.
16. T. Z. Tan, Q. H. Miow, Y. Miki, T. Noda, S. Mori, R. Y. Huang, and J. P. Thiery. Epithelial-mesenchymal transition spectrum quantification and its efficacy in deciphering survival and drug responses of cancer patients. *EMBO Mol Med*, 6(10):1279–1293, Oct 2014.
17. M. Rokavec, M. Kaller, D. Horst, and H. Hermeking. Pan-cancer EMT-signature identifies RBM47 down-regulation during colorectal cancer progression. *Sci Rep*, 7(1):4687, 07 2017.
18. J. S. Parker, M. Mullins, M. C. Cheang, S. Leung, D. Voduc, T. Vickery, S. Davies, C. Fauron, X. He, Z. Hu, J. F. Quackenbush, I. J. Stijleman, J. Palazzo, J. S. Marron, A. B. Nobel, E. Mardis, T. O. Nielsen, M. J. Ellis, C. M. Perou, and P. S. Bernard. Supervised risk predictor of breast cancer based on intrinsic subtypes. *J. Clin. Oncol.*, 27(8):1160–1167, Mar 2009.
19. C. L. Yankaskas, K. N. Thompson, C. D. Paul, M. I. Vitolo, P. Mistriotis, A. Mahendra, V. K. Bajpai, D. J. Shea, K. M. Manto, A. C. Chai, N. Varadarajan, A. Kontrogianni-Konstantopoulos, S. S. Martin, and K. Konstantopoulos. A microfluidic assay for the quantification of the metastatic propensity of breast cancer specimens. *Nat Biomed Eng*, May 2019.
20. W. Chung, H. H. Eum, H. O. Lee, K. M. Lee, H. B. Lee, K. T. Kim, H. S. Ryu, S. Kim, J. E. Lee, Y. H. Park, Z. Kan, W. Han, and W. Y. Park. Single-cell RNA-seq enables comprehensive tumour and immune cell profiling in primary breast cancer. *Nat Commun*, 8:15081, 05 2017.
21. T. S. Andrews and M. Hemberg. False signals induced by single-cell imputation [version 2; peer review: 4 approved]. *F1000Res*, 7:1740, 2019.
22. H. Kennecke, R. Yerushalmi, R. Woods, M. C. Cheang, D. Voduc, C. H. Speers, T. O.

Nielsen, and K. Gelmon. Metastatic behavior of breast cancer subtypes. *J. Clin. Oncol.*, 28 (20):3271–3277, Jul 2010.

23. C. M. Balch, J. E. Gershenwald, S. J. Soong, J. F. Thompson, M. B. Atkins, D. R. Byrd, A. C. Buzaid, A. J. Cochran, D. G. Coit, S. Ding, A. M. Eggermont, K. T. Flaherty, P. A. Gimotty, J. M. Kirkwood, K. M. McMasters, M. C. Mihm, D. L. Morton, M. I. Ross, A. J. Sober, and V. K. Sondak. Final version of 2009 AJCC melanoma staging and classification. *J. Clin. Oncol.*, 27(36):6199–6206, Dec 2009.
24. B. Cieply, P. Riley, P. M. Pifer, J. Widmeyer, J. B. Addison, A. V. Ivanov, J. Denvir, and S. M. Frisch. Suppression of the epithelial-mesenchymal transition by Grainyhead-like-2. *Cancer Res.*, 72(9):2440–2453, May 2012.
25. C. R. Goding and H. Arnheiter. MITF-the first 25 years. *Genes Dev.*, 33(15-16):983–1007, 08 2019.
26. J. Yang, S. A. Mani, J. L. Donaher, S. Ramaswamy, R. A. Itzykson, C. Come, P. Savagner, I. Gitelman, A. Richardson, and R. A. Weinberg. Twist, a master regulator of morphogenesis, plays an essential role in tumor metastasis. *Cell*, 117(7):927–939, Jun 2004.
27. J. T. George, M. K. Jolly, S. Xu, J. A. Somarelli, and H. Levine. Survival Outcomes in Cancer Patients Predicted by a Partial EMT Gene Expression Scoring Metric. *Cancer Res.*, 77(22): 6415–6428, 11 2017.
28. S. Koplev, K. Lin, A. B. Dohlman, and A. Ma'ayan. Integration of pan-cancer transcriptomics with RPPA proteomics reveals mechanisms of epithelial-mesenchymal transition. *PLoS Comput. Biol.*, 14(1):e1005911, 01 2018.
29. T. M. Malta, A. Sokolov, A. J. Gentles, T. Burzykowski, L. Poisson, J. N. Weinstein, and et al. Machine Learning Identifies Stemness Features Associated with Oncogenic Dedifferentiation. *Cell*, 173(2):338–354, 04 2018.
30. D. Jia, J. T. George, S. C. Tripathi, D. L. Kundnani, M. Lu, S. M. Hanash, J. N. Onuchic, M. K. Jolly, and H. Levine. Testing the gene expression classification of the EMT spectrum. *Phys Biol*, 16(2):025002, 01 2019.
31. H. Umeyama, M. Iwadate, and Y. H. Taguchi. TINAGL1 and B3GALNT1 are potential therapy target genes to suppress metastasis in non-small cell lung cancer. *BMC Genomics*, 15 Suppl 9:S2, 2014.
32. D. Sarrio, S. M. Rodriguez-Pinilla, D. Hardisson, A. Cano, G. Moreno-Bueno, and J. Palacios. Epithelial-mesenchymal transition in breast cancer relates to the basal-like phenotype. *Cancer Res.*, 68(4):989–997, Feb 2008.
33. J. Carretero, T. Shimamura, K. Rikova, A. L. Jackson, M. D. Wilkerson, C. L. Borgman, M. S. Buttarazzi, B. A. Sanofsky, K. L. McNamara, K. A. Brandstetter, Z. E. Walton, T. L. Gu, J. C. Silva, K. Crosby, G. I. Shapiro, S. M. Maira, H. Ji, D. H. Castrillon, C. F. Kim, C. Garcia-Echeverria, N. Bardeesy, N. E. Sharpless, N. D. Hayes, W. Y. Kim, J. A. Engelman, and K. K. Wong. Integrative genomic and proteomic analyses identify targets for Lkb1-deficient metastatic lung tumors. *Cancer Cell*, 17(6):547–559, Jun 2010.
34. S. R. Alonso, L. Tracey, P. Ortiz, B. Perez-Gomez, J. Palacios, M. Pollan, J. Linares, S. Serrano, A. I. Saez-Castillo, L. Sanchez, R. Pajares, A. Sanchez-Aguilera, M. J. Artiga, M. A. Piris, and J. L. Rodriguez-Peralto. A high-throughput study in melanoma identifies epithelial-mesenchymal transition as a major determinant of metastasis. *Cancer Res.*, 67(7):3450–3460, Apr 2007.
35. W.-Y. Cheng, J. J. Kandel, D. J. Yamashiro, P. Canoll, and D. Anastassiou. A multi-cancer mesenchymal transition gene expression signature is associated with prolonged time to recurrence in glioblastoma. *PLoS ONE*, 7(4):e34705, April 2012. doi: 10.1371/journal.pone.0034705.
36. J. L. Kaiser, C. L. Bland, and D. J. Klinke. Identifying causal networks linking cancer processes and anti-tumor immunity using Bayesian network inference and metagene constructs. *Biotechnol. Prog.*, 32(2):470–479, 03 2016.
37. S. Davidson, M. Efremova, A. Riedel, B. Mahata, J. Pramanik, J. Huuhtanen, G. Kar, R. Vento-Tormo, T. Hagai, X. Chen, M. A. Haniffa, J. D. Shields, and S. A. Teichmann. Single-cell RNA sequencing reveals a dynamic stromal niche within the evolving tumour microenvironment. *bioRxiv*, 2018. doi: 10.1101/467225.
38. E. Eisenberg and E. Y. Levanon. Human housekeeping genes, revisited. *Trends Genet.*, 29 (10):569–574, Oct 2013.

Figure Legends

Figure 1 - Heatmaps for the expression of a subset of genes in the breast cancer arm of the TCGA study assayed using Illumina RNA-seq (A) and using Agilent microarray (B). Samples obtained from tumor tissue (black) versus matched normal tissue (yellow) are indicated at the bottom of the heatmaps. The genes and samples are similarly ordered in both panels. Values were log2 normalized.

Figure 2 - RPPA measurements were used to determine a threshold for biologically significant changes in gene expression. The model for protein dependence on gene expression (A) where representative data (black circles) and model fits (dotted black line) are shown for CLDN7, AXL, JAG1, and CDH1 (B). (C) The distribution in threshold values calculated for all 147 genes. In (B), the vertical red dotted line indicates the threshold value and the melanoma and breast cancer cell lines are highlighted by red and blue circles.

Figure 3 - Data workflow for identifying epithelial/differentiated versus mesenchymal/de-differentiated state metrics. Workflow contains three decision points: unsupervised feature extraction (FE)/feature selection (FS) based on PCA, a binary fibroblast filter, and a consistency filter based on Ridge logistic regression of annotated samples.

Figure 4 - Two opposing gene signatures were identified among the cohort of breast cancer cell lines. (A) Scree plot of the percentage of variance explained by each principal component, where the dotted line corresponds to variance explained by the null principal components. (B) Projection of the genes along PC1 and PC2 axes, where the font color corresponds to the mean read counts among cell lines (blue-yellow-red corresponds to high-medium-low read counts). (C) Projection of the genes along PC2 and PC3 axes, where the dotted lines enclose 90% of the null PCA distribution along the corresponding axis.

Figure 5 - The different subsets of breast cancer were clustered along a reciprocal epithelial to mesenchymal state axes. Log2 projections along the epithelial (SM_E) and mesenchymal (SM_M) state axes for each breast cancer cell line included in the CCLE (A) and primary breast cancer cells (B and C). Values for SM_E and SM_M were estimated by bulk RNA-seq data for cell lines associated with the CCLE and by scRNA-seq data for primary tumor cells (20). (C) Log2 state projections are compared for primary breast cancer cells as originally reported and with dropout values imputed using the values averaged over the rest of the sample population, where grey lines connect the original state values to state values determine after imputation. Symbols were colored based on previously annotated breast cancer PAM50 subtypes: basal - red, claudin low - yellow, HER2 - pink, luminal A - blue, luminal B - black. In panel A, the metastatic potential of a subset of cell lines were annotated based on a recent study (19): low metastatic potential - grey circle, high metastatic potential - red circle. The dotted line corresponds to a reciprocal relationship between the SM_E and SM_M state metrics (i.e., SM_E = 1 - SM_M).

Figure 6 - The samples from normal breast tissue and breast cancer were clustered separately along a reciprocal epithelial to mesenchymal state axes. Using EMT genes that passed the gene filter workflow, each sample contained within the breast cancer (BrCa) arm of the TCGA was projected along the epithelial (SM_E) versus mesenchymal (SM_M) state axes using the corresponding bulk RNA-seq data. Symbols were colored based on normal breast tissue (green) or clinical breast cancer subtype: ER/PR+ - blue, HER2 - pink, triple negative (TN) - red. The dotted line corresponds to a reciprocal relationship between the SM_E and SM_M state metrics (i.e., SM_E = 1 - SM_M).

Figure 7 - Two opposing gene signatures were identified among the cohort of melanoma cell lines. (A) Scree plot of the percentage of variance explained by each principal component, where the dotted line corresponds to variance explained by the null principal components. (B) Projection of the genes along PC1 and PC2 axes, where the font color corresponds to the mean read counts among cell lines (blue-yellow-red corresponds to high-medium-low read counts). (C) Projection of the genes along PC2 and PC3 axes, where the dotted lines enclose 90% of the null PCA distribution along the corresponding axis.

Figure 8 - Melanoma cell lines and primary single melanoma cells are distributed along path between extremes in differentiation states. Projections along the terminally differentiated (SM_T) versus de-differentiated (SM_D) state axes for each melanoma cell line included in the CCLE (A) and primary melanoma cells (B). Values for the terminally differentiated and de-differentiated state metrics were estimated by RNA-seq data for cell lines associated with the CCLE and by scRNA-seq data for primary melanoma cells. Symbols for primary melanoma cells were colored differently for each patient sample. The dotted line corresponds to a reciprocal relationship between the SM_T and SM_D state metrics (i.e., SM_T = 1 - SM_D).

Figure 9 - Gene expression patterns associated with benign melanocytic nevi and primary melanoma tissue samples are distributed along path between extremes in differentiation states. Projections along the terminally differentiated (SM_T) versus de-differentiated (SM_D) state axes for 78 tissue samples obtained from common acquired melanocytic nevi (n = 27, green circles) and primary melanoma (n = 51). The primary melanoma samples are colored based on the Breslow's depth (blue: 0.1 mm to red: 10+ mm). The dotted line corresponds to a reciprocal relationship between the SM_T and SM_D state metrics (i.e., SM_T = 1 - SM_D).

Figure 10 - Venn diagram illustrating overlap in genes contained in the opposing state metrics for terminally differentiated/epithelial versus de-differentiated/mesenchymal extracted from breast cancer (blue circle) and melanoma (red circle) cell lines. The subset of the genes listed below the Venn diagram were annotated with transcription factor GO terms.

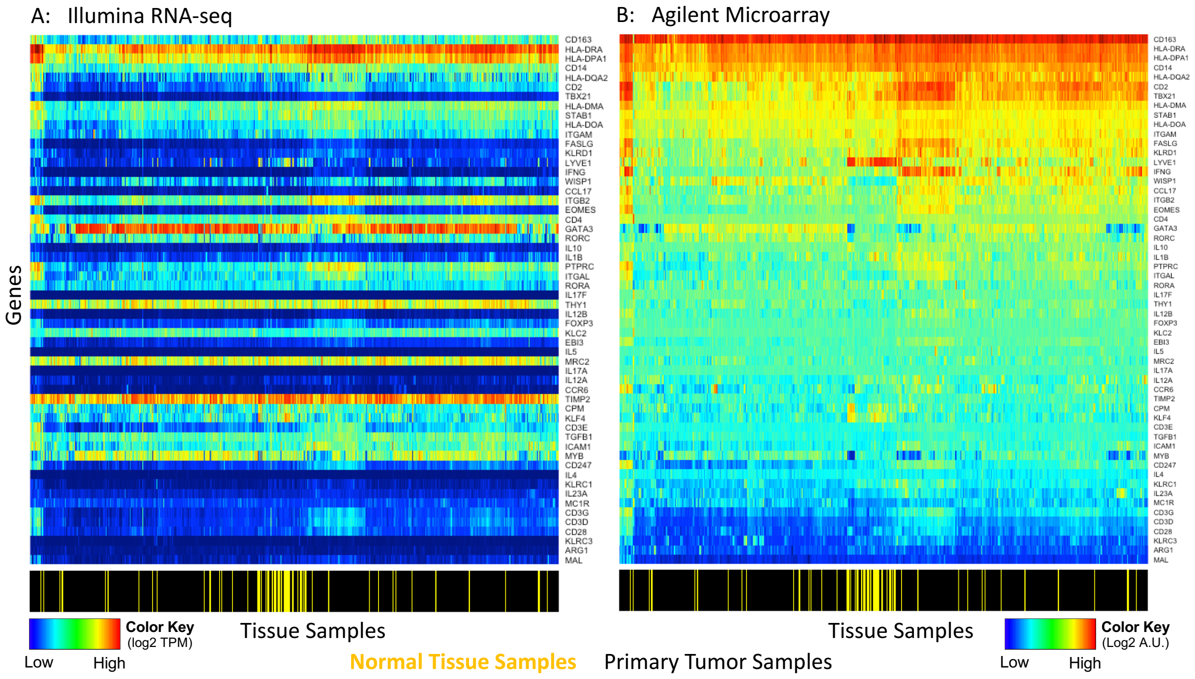

Fig. 1. Heatmaps for the expression of a subset of genes in the breast cancer arm of the TCGA study assayed using Illumina RNA-seq (A) and using Agilent microarray (B). Samples obtained from tumor tissue (black) versus matched normal tissue (yellow) are indicated at the bottom of the heatmaps. The genes and samples are similarly ordered in both panels. Values were log2 normalized.

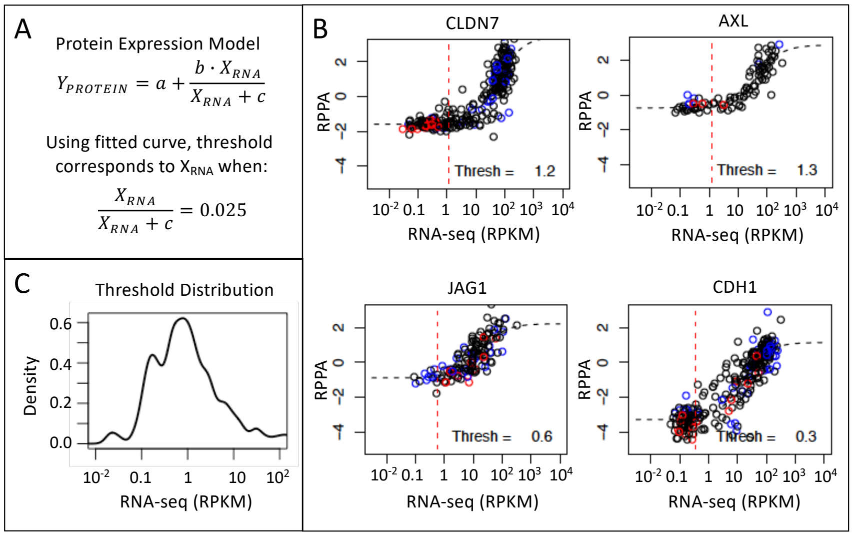

Fig. 2. RPPA measurements were used to determine a threshold for biologically significant changes in gene expression. The model for protein dependence on gene expression (A) where representative data (black circles) and model fits (dotted black line) are shown for CLDN7, AXL, JAG1, and CDH1 (B). (C) The distribution in threshold values calculated for all 147 genes. In (B), the vertical red dotted line indicates the threshold value and the melanoma and breast cancer cell lines are highlighted by red and blue circles.

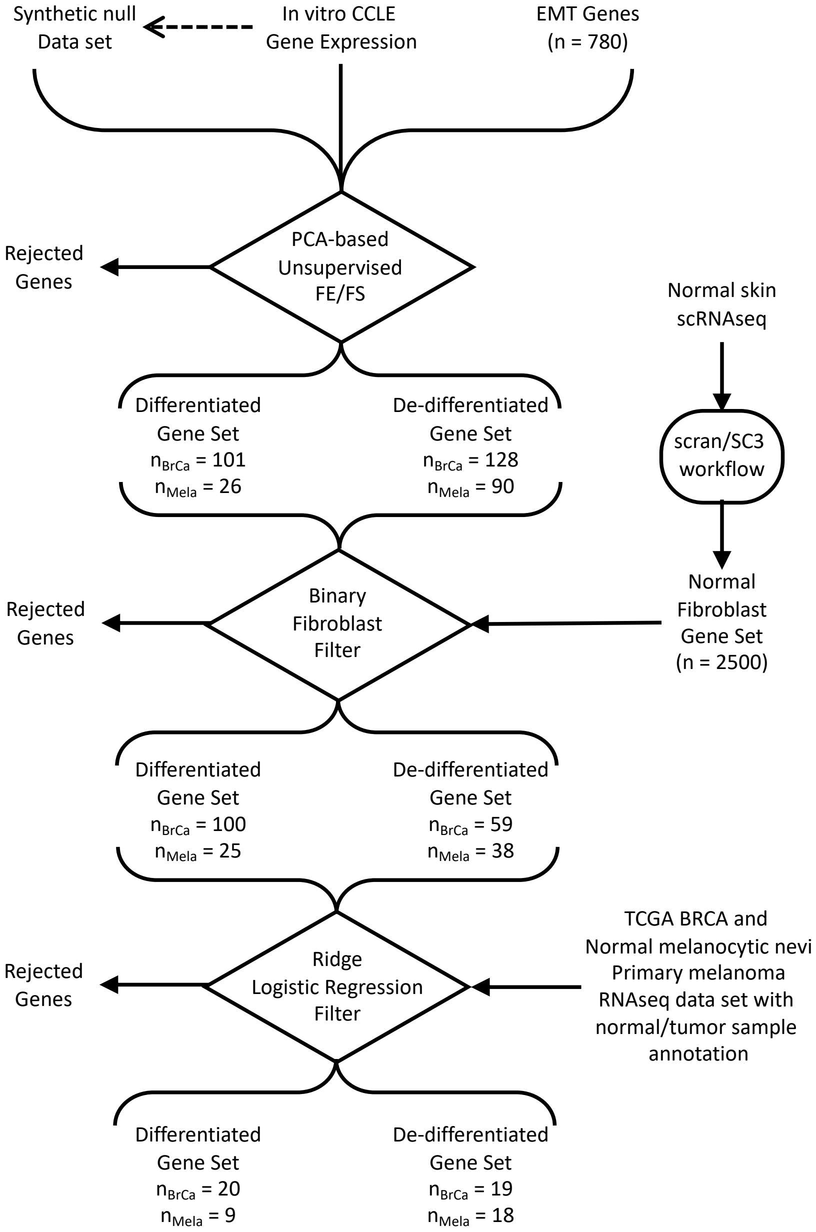
Synthetic null Data set
In vitro CCLE Gene Expression
EMT Genes (n = 780)
PCA-based Unsupervised FE/FS
Rejected Genes
Normal skin scRNAseq
scran/SC3 workflow
Differentiated Gene Set n_{BrCa} = 101 n_{Mela} = 26
De-differentiated Gene Set n_{BrCa} = 128 n_{Mela} = 90
Binary Fibroblast Filter
Rejected Genes
Normal Fibroblast Gene Set (n = 2500)
Differentiated Gene Set n_{BrCa} = 100 n_{Mela} = 25
De-differentiated Gene Set n_{BrCa} = 59 n_{Mela} = 38
Ridge Logistic Regression Filter
Rejected Genes
TCGA BRCA and Normal melanocytic nevi Primary melanoma RNAseq data set with normal/tumor sample annotation
Differentiated Gene Set n_{BrCa} = 20 n_{Mela} = 9
De-differentiated Gene Set n_{BrCa} = 19 n_{Mela} = 18

Fig. 3. Data workflow for identifying epithelial/differentiated versus mesenchymal/de-differentiated state metrics. Workflow contains three decision points: unsupervised feature extraction (FE)/feature selection (FS) based on PCA, a binary fibroblast filter, and a consistency filter based on Ridge logistic regression of annotated samples.

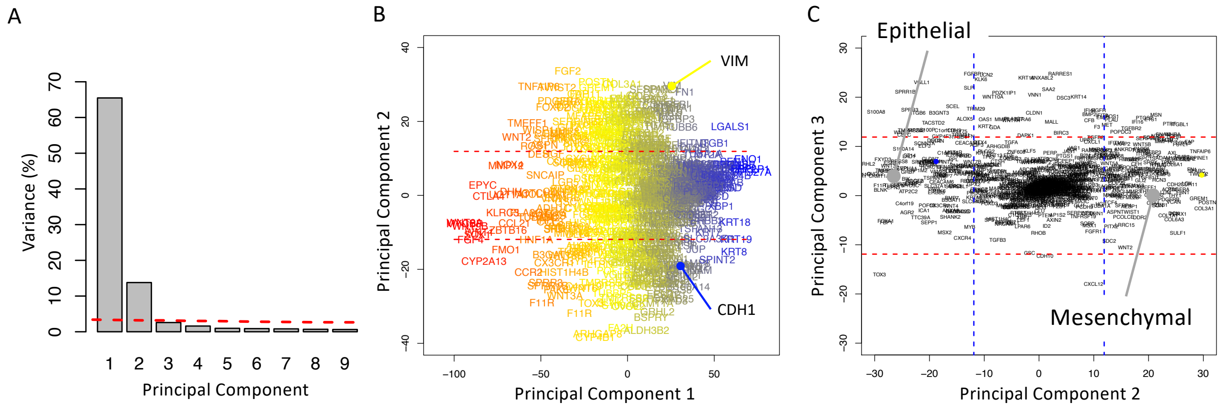

Fig. 4. Two opposing gene signatures were identified among the cohort of breast cancer cell lines. (A) Scree plot of the percentage of variance explained by each principal component, where the dotted line corresponds to variance explained by the null principal components. (B) Projection of the genes along PC1 and PC2 axes, where the font color corresponds to the mean read counts among cell lines (blue-yellow-red corresponds to high-medium-low read counts). (C) Projection of the genes along PC2 and PC3 axes, where the dotted lines enclose 90% of the null PCA distribution along the corresponding axis. .

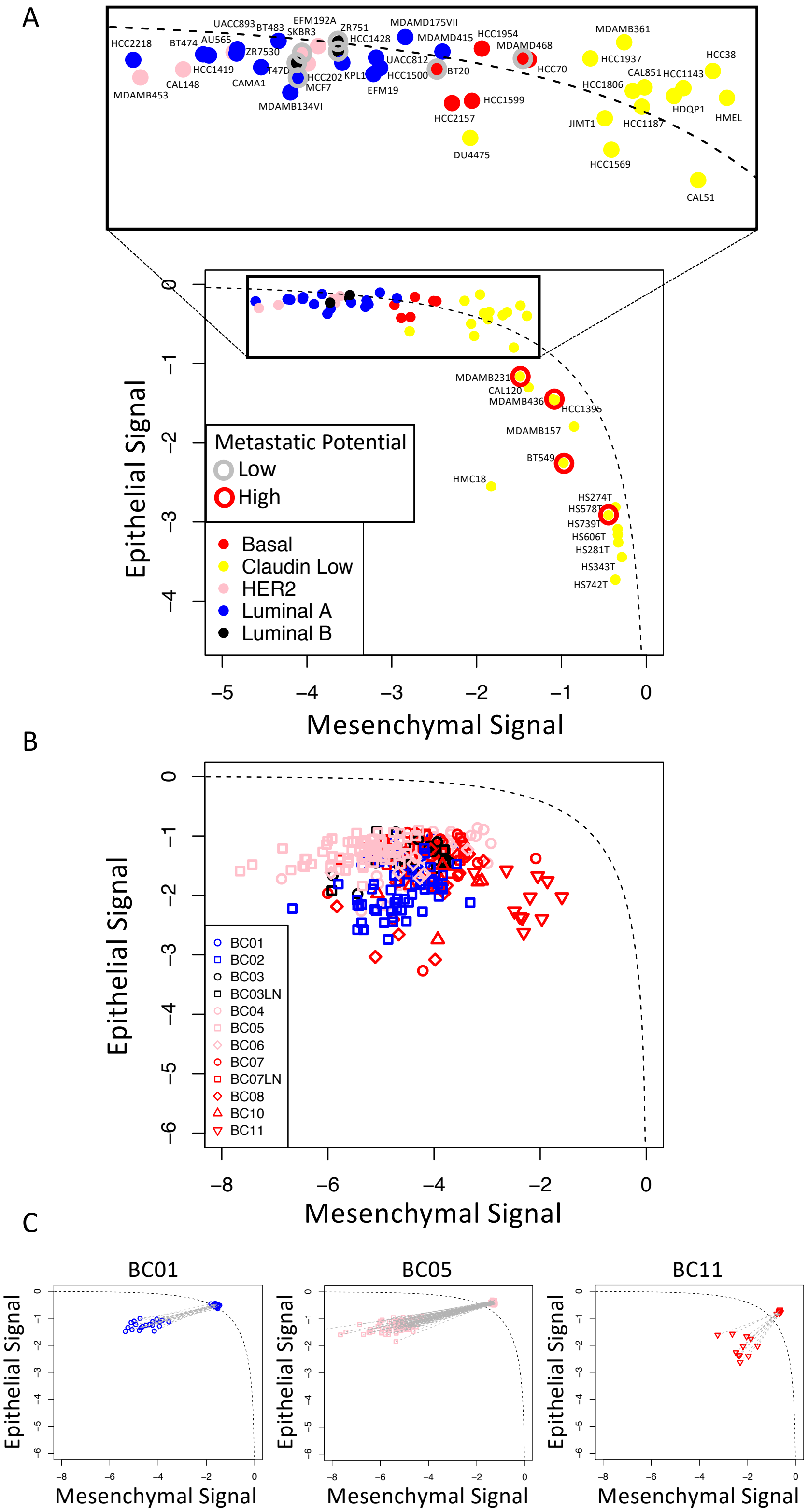

Fig. 5. The different subsets of breast cancer were clustered along a reciprocal epithelial to mesenchymal axes. Log2 projections along the epithelial (SM_E) and mesenchymal (SM_M) state axes for each breast cancer cell line included in the CCLE (A) and primary breast cancer cells (B and C). Values for SM_E and SM_M were estimated by bulk RNA-seq data for cell lines associated with the CCLE and by scRNA-seq data for primary tumor cells (20). (C) Log2 state projections are compared for primary breast cancer cells as originally reported and with dropout values imputed using the values averaged over the rest of the sample population, where grey lines connect the original state values to state values determine after imputation. Symbols were colored based on previously annotated breast cancer PAM50 subtypes: basal - red, claudin low - yellow, HER2 - pink, luminal A - blue, luminal B - black. In panel A, the metastatic potential of a subset of cell lines were annotated based on a recent study (19): low metastatic potential - grey circle, high metastatic potential - red circle. The dotted line corresponds to a reciprocal relationship between the SM_E and SM_M state metrics (i.e., SM_E = 1 - SM_M).

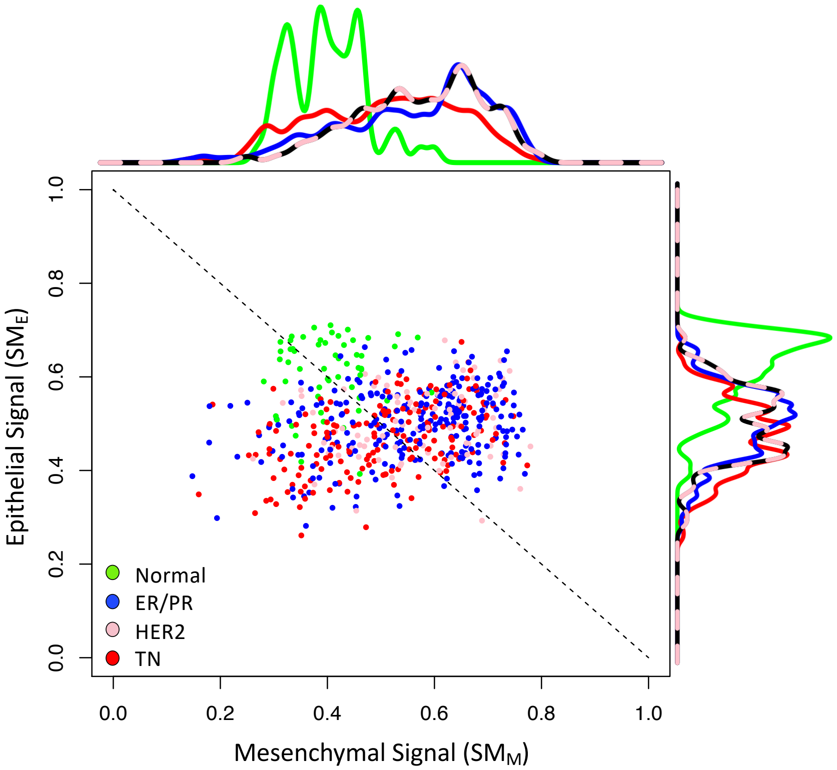

Fig. 6. The samples from normal breast tissue and breast cancer were clustered separately along a reciprocal epithelial to mesenchymal state axes. Using EMT genes that passed the gene filter workflow, each sample contained within the breast cancer (BrCa) arm of the TCGA was projected along the epithelial (SM_E) versus mesenchymal (SM_M) state axes using the corresponding bulk RNA-seq data. Symbols were colored based on normal breast tissue (green) or clinical breast cancer subtype: ER/PR+ - blue, HER2 - pink, triple negative (TN) - red. The dotted line corresponds to a reciprocal relationship between the SM_E and SM_M state metrics (i.e., SM_E = 1 - SM_M).

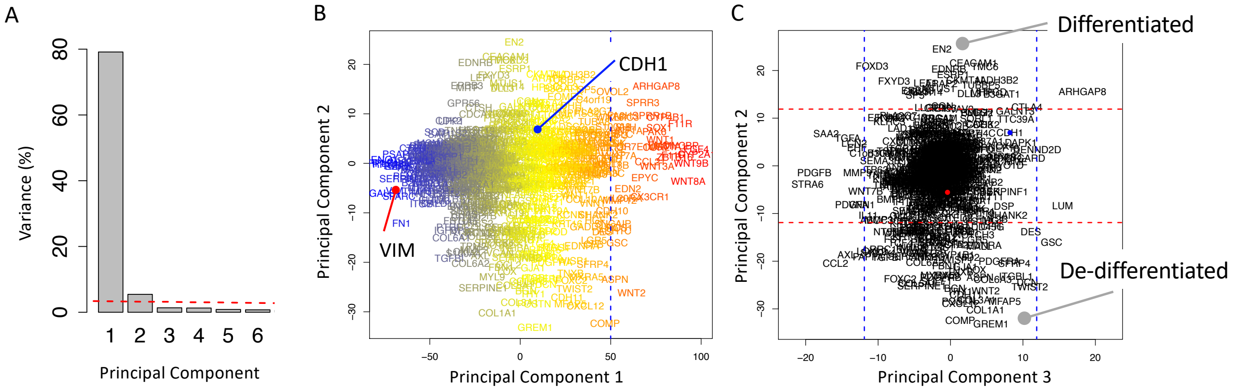

Fig. 7. Two opposing gene signatures were identified among the cohort of melanoma cell lines. (A) Scree plot of the percentage of variance explained by each principal component, where the dotted line corresponds to variance explained by the null principal components. (B) Projection of the genes along PC1 and PC2 axes, where the font color corresponds to the mean read counts among cell lines (blue-yellow-red corresponds to high-medium-low read counts). (C) Projection of the genes along PC2 and PC3 axes, where the dotted lines enclose 90% of the null PCA distribution along the corresponding axis.

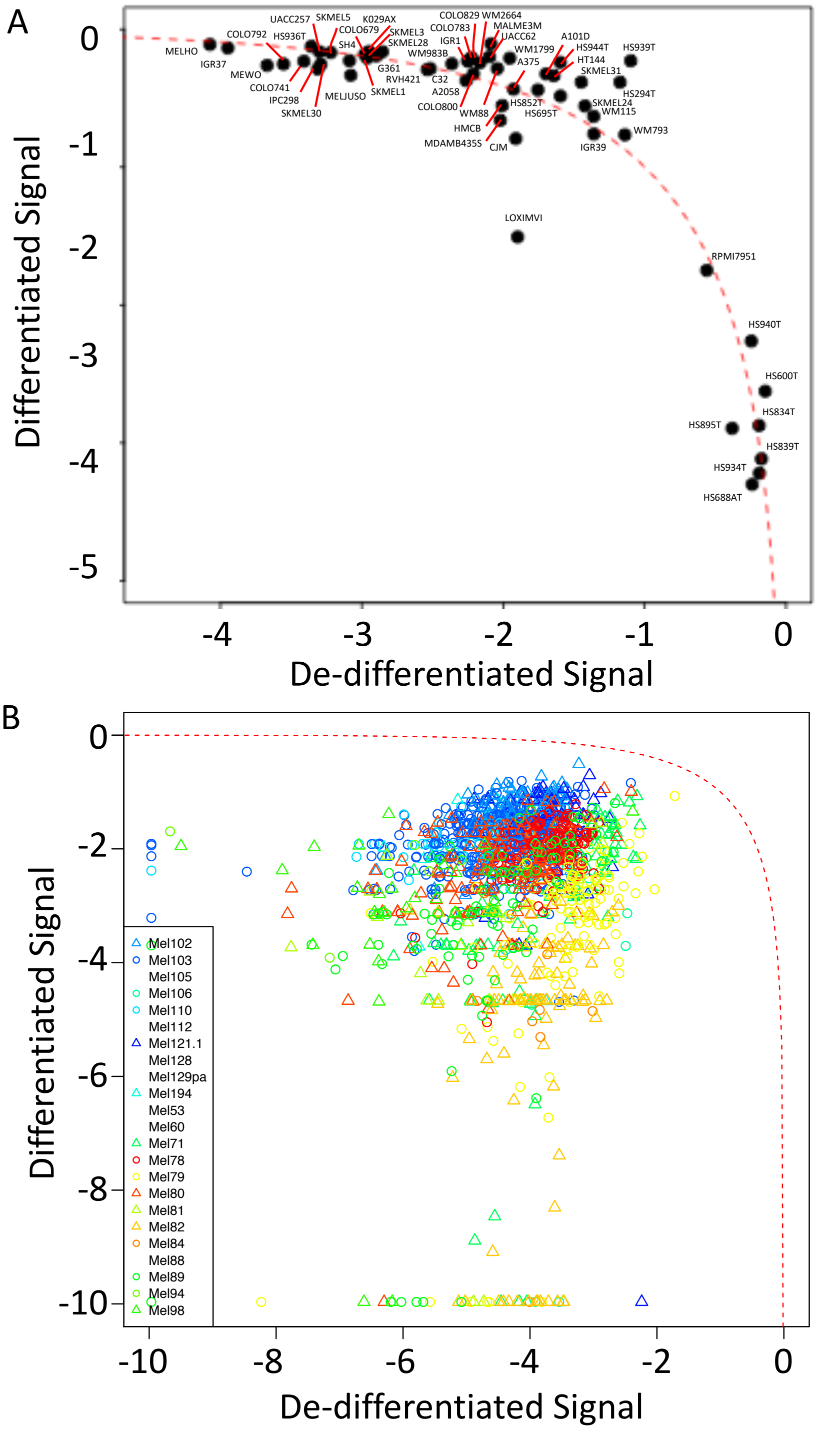

Fig. 8. Melanoma cell lines and primary single melanoma cells are distributed along path between extremes in differentiation states. Projections along the terminally differentiated (SM_T) versus de-differentiated (SM_D) state axes for each melanoma cell line included in the CCLE (A) and primary melanoma cells (B). Values for the terminally differentiated and de-differentiated state metrics were estimated by RNA-seq data for cell lines associated with the CCLE and by scRNA-seq data for primary melanoma cells. Symbols for primary melanoma cells were colored differently for each patient sample. The dotted line corresponds to a reciprocal relationship between the SM_T and SM_D state metrics (i.e., SM_T = 1 - SM_D).

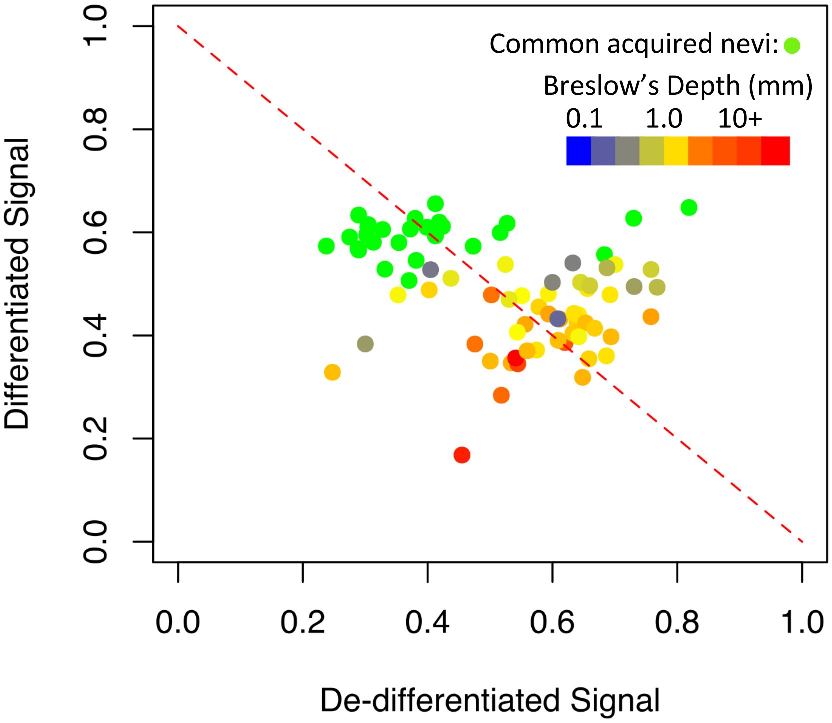

Fig. 9. Gene expression patterns associated with benign melanocytic nevi and primary melanoma tissue samples are distributed along path between extremes in differentiation states. Projections along the terminally differentiated (SM_T) versus de-differentiated (SM_D) state axes for 78 tissue samples obtained from common acquired melanocytic nevi (n = 27, green circles) and primary melanoma (n = 51). The primary melanoma samples are colored based on the Breslow's depth (blue: 0.1 mm to red: 10+ mm). The dotted line corresponds to a reciprocal relationship between the SM_T and SM_D state metrics (i.e., SM_T = 1 - SM_D).

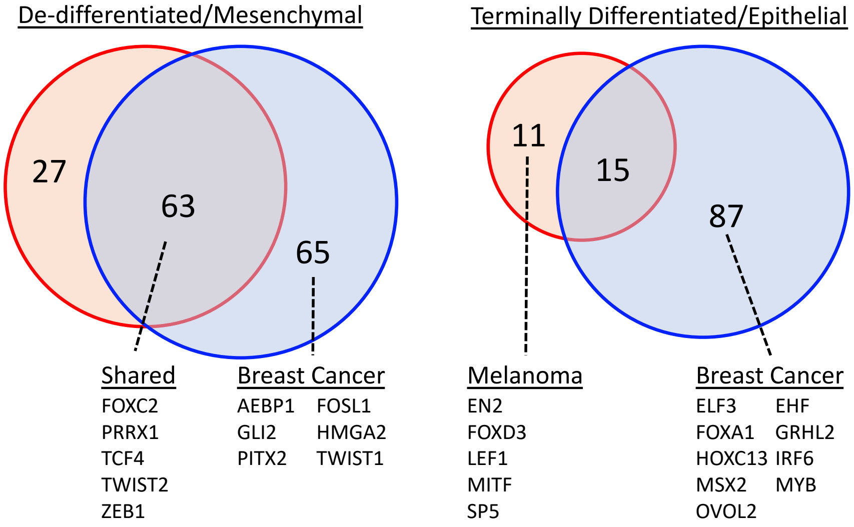

Fig. 10. Venn diagram illustrating overlap in genes contained in the opposing state metrics for terminally differentiated/epithelial versus de-differentiated/mesenchymal extracted from breast cancer (blue circle) and melanoma (red circle) cell lines. The subset of the genes listed below the Venn diagram were annotated with transcription factor GO terms.

Supplemental Table S1: List of genes and associated Ki values for state metrics developed separately for breast cancer and melanoma cell lines based on CCLE gene expression. Genes that overlap with the fibroblast gene list are highlighted in yellow.

Breast Cancer Cell Lines							
Epithelial Signature				Mesenchymal Signature			
GENE_SYMBOL	*Ki (log2 RPKM)*	GENE_SYMBOL	*Ki (log2 RPKM)*	GENE_SYMBOL	*Ki (log2 RPKM)*	GENE_SYMBOL	*Ki (log2 RPKM)*
AGR2	4.303	MSX2	0.179	ACTA2	4.645	LRRC15	-1.540
ALDH3B2	0.520	MYB	1.005	ADAM12	1.213	LUM	2.397
ANK3	1.913	MYH14	0.824	AEBP1	1.713	MAP1B	2.978
ANXA9	0.578	MYO5C	0.331	AKAP12	2.053	MFAP5	2.074
AP1M2	2.493	OCLN	1.859	AKAP2	3.118	MME	1.766
ARAP2	-0.552	OR7E14P	-2.318	AKT3	0.416	MMP14	3.304
ARHGAP8	1.490	OVOL2	-1.155	ANK2	0.601	MMP2	3.829
ATP2C2	0.658	PDGFB	-0.006	ANKRD1	1.447	MMP3	-0.991
B3GAT1	-4.481	PKP3	3.550	ASPN	-2.623	MXRA7	5.608
BIK	-0.863	POF1B	-1.516	AXL	2.334	MYL9	5.899
BLNK	-1.428	PPL	1.218	BAG2	3.569	NID2	2.901
BMP7	0.620	PRSS8	1.555	BGN	3.131	OLFML2B	1.328
BSPRY	-0.611	PTK6	0.001	C1S	3.335	PAPPA	-0.115
C1orf106	0.560	RAB25	2.438	C7orf10	1.725	PCOLCE	5.904
C4orf19	-0.366	RBM47	2.246	CALD1	6.281	PDGFC	3.280
CDH1	2.795	S100A14	4.046	CCL2	1.510	PDGFRA	-0.202
CDS1	1.006	SCNN1A	1.824	CD68	3.038	PDGFRB	0.881
CEACAM1	-0.966	SEPP1	0.991	CDH11	1.460	PHLDA1	4.056
CEACAM6	1.792	SH2D3A	1.585	CDH2	2.593	PITX2	-0.019
CGN	1.288	SHANK2	2.091	CFH	0.413	PLAUR	4.775
CKMT1A	0.521	SLC37A1	1.335	CLIC4	6.784	PMP22	4.088
CLDN4	3.878	SORL1	0.433	COL1A1	7.342	POSTN	2.347
CLDN7	3.118	SPINT1	2.939	COL3A1	4.258	PROCR	2.922
CNKSR1	1.476	SPINT2	5.621	COL5A1	4.259	PRRX1	1.135
CX3CR1	-4.771	ST14	1.517	COL5A2	3.450	RCN3	4.002
CXCR4	0.197	TMC6	2.345	COL6A1	4.820	RECK	1.117
CYP4B1	-2.086	TMPRSS2	-0.925	COL6A2	4.411	S100A4	6.135
DENND2D	1.285	TSPAN1	2.975	COL6A3	3.274	SACS	2.466
DSC2	-0.117	TSPAN15	2.498	COMP	-2.248	SDC2	5.076
EDN2	-0.828	TTC39A	1.812	COPZ2	3.117	SERPINB2	1.275
EFNA1	2.368	TUBBP5	-2.023	CTSB	8.252	SERPINE1	5.902
EHF	1.234	VAMP8	3.649	CXCL3	-0.315	SERPINE2	5.411
ELF3	3.414	VAV3	0.658	CYBRD1	3.701	SFRP4	-1.523
EPCAM	3.550	WNT3A	-4.542	DAB2	3.127	SH3KBP1	3.938
EPHA1	1.955	WNT4	-1.102	DCN	2.442	SMARCA1	3.121
EPN3	1.083	WNT7B	1.009	DDR2	2.484	SPARC	6.576
EPS8L1	3.622			EDNRA	-1.472	SPOCK1	3.964
ERBB3	2.885			EMP3	5.080	SRPX	2.604
ESRP1	1.288			FAP	1.059	SULF1	2.944
ESRP2	1.782			FBN1	4.146	TCF4	0.705
EVPL	0.234			FGF1	-0.793	TFPI	2.062
EXPH5	-0.989			FHL1	2.511	TGFB1	4.092
F11R	3.294			FN1	8.443	TGFB1I1	3.009
FA2H	-1.889			FOSL1	3.395	THBS2	1.126
FBP1	1.225			FOXC2	-2.174	THY1	3.625
FOXA1	1.528			FST	2.555	TIMP3	3.708
FXYD3	4.244			FSTL1	6.206	TMEFF1	0.365
GADD45G	0.490			GAS1	-0.239	TMEM158	1.520
GALNT3	1.907			GEM	2.394	TNC	3.234
GPX2	-0.492			GFPT2	1.976	TNFAIP6	-0.824
GRB7	1.676			GJA1	2.267	TPM2	6.350
GRHL2	0.121			GLI2	-0.830	TRPC1	1.437
HOXC13	0.223			GLT8D2	1.557	TUBB6	7.243
HPGD	-2.173			GREM1	2.165	TWIST1	-0.148
ICA1	1.509			HMGA2	1.081	TWIST2	-2.302
IL1RN	-1.966			HTRA1	4.465	VCAN	2.709
IL20RA	-1.730			IFITM3	6.742	VEGFC	3.036
IRF6	0.688			IGFBP3	6.102	VIM	7.107
JUP	4.203			ITGA5	5.433	WISP1	-1.528
KRT8	7.266			ITGB1	9.185	WNT2	-3.475
LAD1	1.200			LEPRE1	5.248	WNT5A	2.457
LLGL2	2.833			LGALS1	10.947	WNT5B	1.454
LSR	3.936			LHFP	2.623	ZEB1	1.196
MAP7	1.737			LOX	3.766		
MST1R	1.087			LOXL2	5.430		

Melanoma Cell Lines					
Differentiated Signature		Dedifferentiated Signature			
GENE_SYMBOL	*Ki (log2 RPKM)*	GENE_SYMBOL	*Ki (log2 RPKM)*	GENE_SYMBOL	*Ki (log2 RPKM)*
ALDH3B2	-5.189	ACTA2	3.745	PTGS1	-0.242
ARAP2	-4.050	ADAM12	2.139	PTRF	6.629
B3GAT1	-4.604	ANKRD1	1.628	RCN3	4.772
BIK	-2.759	ASPN	-3.222	RHOD	-0.186
CCL3	-5.000	BGN	2.914	S100A4	5.840
CEACAM1	-1.634	C1S	3.186	SERPINB2	2.400
CGN	-2.178	CDH11	0.196	SERPINE1	5.626
CKMT1A	-3.799	CFB	-2.397	SFRP4	-2.295
CTLA4	-3.172	CFH	0.952	SPOCK1	3.602
DLL3	-0.614	CLU	2.266	SULF1	1.976
EDNRB	0.359	COL1A1	5.727	TCF4	0.102
EN2	-2.698	COL3A1	3.561	TFPI	1.789
ERBB3	1.506	COL5A1	3.086	TGFBI	7.149
ESRP1	-1.928	COL5A2	4.597	THBS2	4.502
FOXD3	-2.372	COL6A1	6.709	THY1	2.529
FXYD3	-0.741	COL6A2	5.868	TNXB	-0.760
GPR56	2.428	COL6A3	2.436	TPM2	5.480
HPGD	-3.570	COMP	-1.689	TWIST2	-0.122
LEF1	0.291	CXCL12	-0.942	VCAN	3.364
LLGL2	-2.142	CYP1B1	0.958	VEGFC	2.386
MITF	2.097	DCN	1.695	WISP1	-1.139
MTUS1	-1.067	DES	-3.426	WNT2	-4.060
MYH14	-1.413	EDNRA	-2.070	WNT5A	2.285
SP5	-6.085	EGFR	1.402	WNT5B	1.010
TMC6	-0.954	EPS8L2	0.890	ZEB1	1.984
TUBBP5	-4.963	FAP	3.289		
		FBN1	3.869		
		FGF1	0.675		
		FGF2	2.188		
		FHL1	3.489		
		FN1	9.974		
		FOXC2	-0.834		
		FST	3.630		
		GADD45G	-3.399		
		GJA1	1.946		
		GLT8D2	0.526		
		GREM1	3.220		
		IFITM2	4.612		
		IGFBP3	6.190		
		IL1R1	1.252		
		INHBA	2.436		
		ITGBL1	2.227		
		KRT14	1.237		
		KRT16	-1.959		
		KRT7	1.856		
		LGR5	-3.329		
		LOX	3.878		
		LOXL2	5.806		
		LRRC15	-0.003		
		MALL	0.019		
		MFAP5	0.136		
		MMP2	5.236		
		MXRA5	-1.889		
		MYL9	4.994		
		NID2	1.253		
		NOTCH3	1.644		
		NT5E	5.491		
		PAPPA	-0.187		
		PCOLCE	4.551		
		PDGFC	1.425		
		PDGFRA	0.445		
		PDGFRB	1.315		
		PLAU	2.161		
		POSTN	2.399		
		PRRX1	2.462		

Table S1. List of genes and corresponding K_i values for state metrics developed separately for breast cancer and melanoma cell lines based on CCLE gene expression. Genes that overlap with the fibroblast gene list are highlighted in yellow.

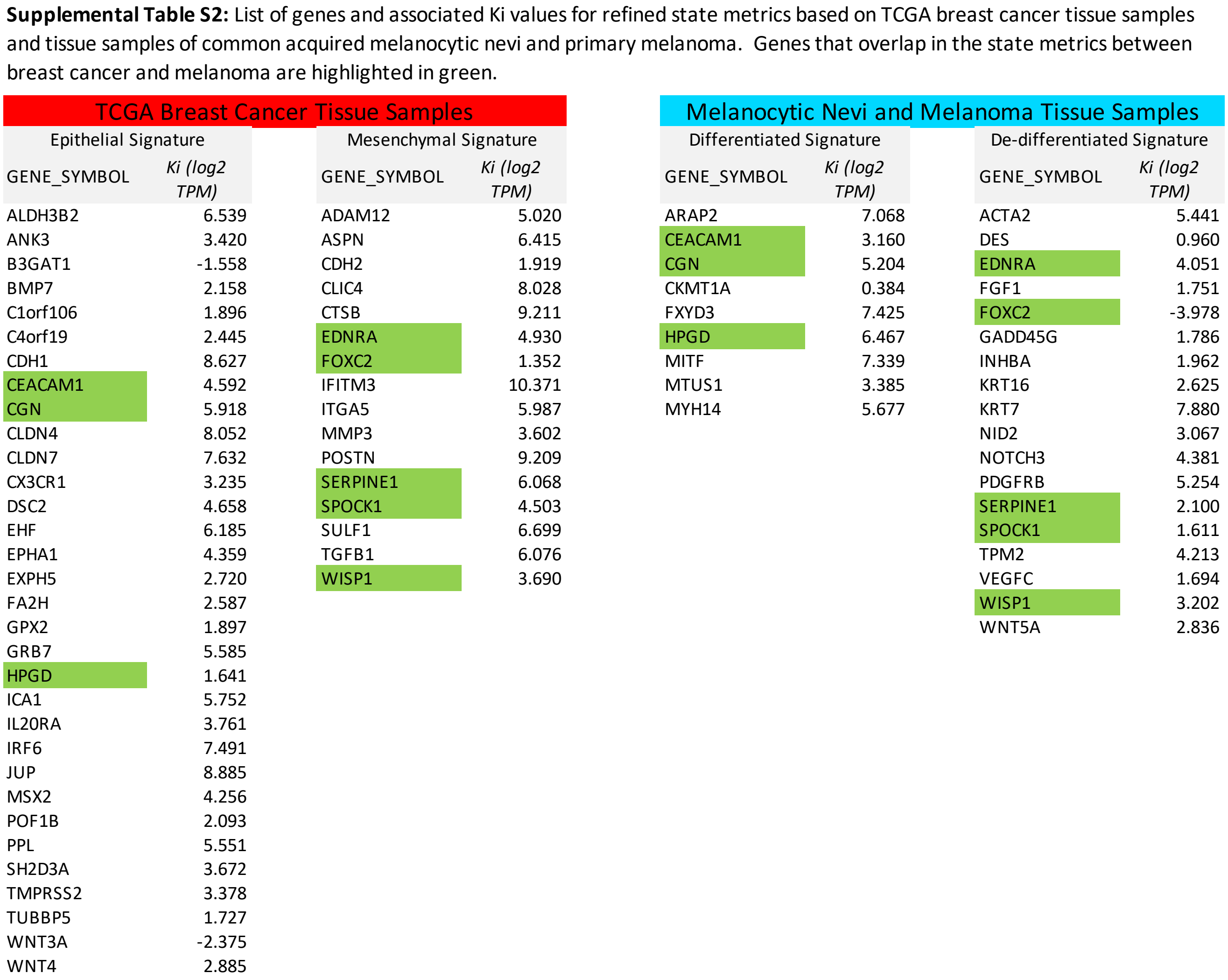

Supplemental Table S2: List of genes and associated Ki values for refined state metrics based on TCGA breast cancer tissue samples and tissue samples of common acquired melanocytic nevi and primary melanoma. Genes that overlap in the state metrics between breast cancer and melanoma are highlighted in green.

TCGA Breast Cancer Tissue Samples				Melanocytic Nevi and Melanoma Tissue Samples			
Epithelial Signature		Mesenchymal Signature		Differentiated Signature		De-differentiated Signature	
GENE_SYMBOL	*Ki (log2 TPM)*	GENE_SYMBOL	*Ki (log2 TPM)*	GENE_SYMBOL	*Ki (log2 TPM)*	GENE_SYMBOL	*Ki (log2 TPM)*
ALDH3B2	6.539	ADAM12	5.020	ARAP2	7.068	ACTA2	5.441
ANK3	3.420	ASPN	6.415	CEACAM1	3.160	DES	0.960
B3GAT1	-1.558	CDH2	1.919	CGN	5.204	EDNRA	4.051
BMP7	2.158	CLIC4	8.028	CKMT1A	0.384	FGF1	1.751
C1orf106	1.896	CTSB	9.211	FXYD3	7.425	FOXC2	-3.978
C4orf19	2.445	EDNRA	4.930	HPGD	6.467	GADD45G	1.786
CDH1	8.627	FOXC2	1.352	MITF	7.339	INHBA	1.962
CEACAM1	4.592	IFITM3	10.371	MTUS1	3.385	KRT16	2.625
CGN	5.918	ITGA5	5.987	MYH14	5.677	KRT7	7.880
CLDN4	8.052	MMP3	3.602			NID2	3.067
CLDN7	7.632	POSTN	9.209			NOTCH3	4.381
CX3CR1	3.235	SERPINE1	6.068			PDGFRB	5.254
DSC2	4.658	SPOCK1	4.503			SERPINE1	2.100
EHF	6.185	SULF1	6.699			SPOCK1	1.611
EPHA1	4.359	TGFB1	6.076			TPM2	4.213
EXPH5	2.720	WISP1	3.690			VEGFC	1.694
FA2H	2.587					WISP1	3.202
GPX2	1.897					WNT5A	2.836
GRB7	5.585						
HPGD	1.641						
ICA1	5.752						
IL20RA	3.761						
IRF6	7.491						
JUP	8.885						
MSX2	4.256						
POF1B	2.093						
PPL	5.551						
SH2D3A	3.672						
TMPRSS2	3.378						
TUBBP5	1.727						
WNT3A	-2.375						
WNT4	2.885						

Table S2. List of genes and associated Ki values for refined state metrics based on TCGA breast cancer tissue samples and tissue samples of common acquired melanocytic nevi and primary melanoma. Genes that overlap in the state metrics between breast cancer and melanoma are highlighted in green.

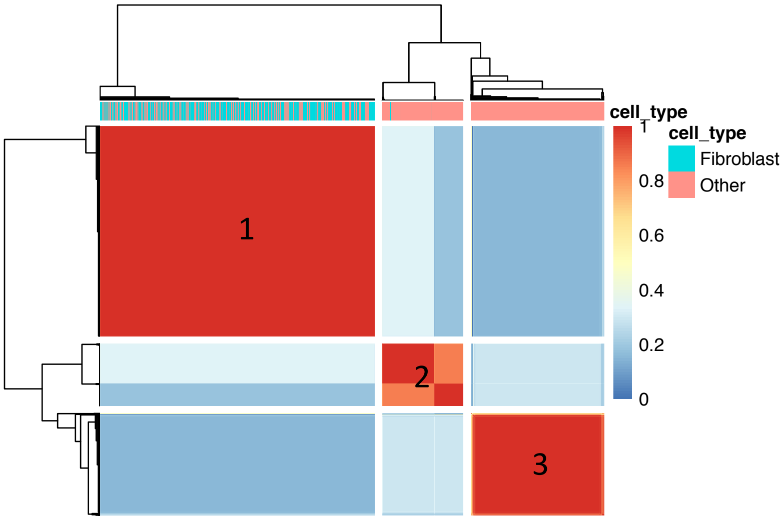

Fig. S1. Consensus matrix for similarity and clustering of cell samples. The symmetric 1034x1034 matrix is colored in element(i,j) by similarity in assigning cells i and j to the same cluster when the clustering parameters are changed. A similarity score of 0 (blue) indicates that the two cells are always assigned to different clusters while a score of 1 (red) indicates that the two cells are always assigned to the same cluster. The similarity of the samples are also illustrated by the dendrograms shown on the top and side. The top bar indicates whether the cell was annotated as a fibroblast based on COL1A1 and COL1A2 expression (aqua – fibroblast, pink – other).